# On the translation of a cylinder in a long tube

Hui Liu, Haim H. Bau,[a] and Howard Hu
*Department of Mechanical Engineering and Applied Mechanics, University of Pennsylvania, Philadelphia, Pennsylvania 19104-6315*

(Received 27 November 2002; accepted 10 October 2003; published online 8 March 2004)

We study the motion of a cylindrical particle translating slowly in a long tube as a function of the particle's dimensions and placement both in the presence and the absence of external pressure gradients. The cylinder acts as a ''leaky'' piston, generating both fluid recirculation and through flow. When the particle is long, analytic expressions are obtained for both the velocity field and the force needed to sustain the particle's motion as functions of the particle's position and dimensions. When the particle is short, a superposition-based algorithm is outlined to facilitate economical numerical calculations. When the particle is placed off center in the tube, torque will act on the particle. When the particle is unguided, this torque will preclude coaxial motion and cause the particle to follow an oscillatory trajectory. © *2004 American Institute of Physics.*
[DOI: 10.1063/1.1650334]

## I. INTRODUCTION

Our study of the motion of a cylindrical particle in a tube is motivated by the desire to estimate the hydrodynamic forces acting on macromolecules or nanocylinders translating in small diameter tubes. To the first order approximation, we consider the macromolecule to be a rigid cylinder. The cylinder is subjected to an external field such as a gravitational or electromagnetic field. We assume that the particle's axis is parallel to, but not necessarily co-aligned with, the tube's axis. As the cylinder translates in the tube, it drags fluid with it, acting as a leaky piston. The cylinder may induce both recirculating and net (through) flows. We wish to determine the forces that act on the cylinder. This knowledge may be useful, among other things, for analyzing sensors in which macromolecules are transmitted through small tubes, needle-type viscometers operating with Newtonian fluids, and cylindrical capsules moving in microfluidic devices.

Most of the studies to date have been motivated by the needle viscometer and have focused on long, axisymmetrically[1–3] and eccentrically[4,5] translating cylinders in closed tubes. Davis[6] approximated the finite cylinder as an array of equally spaced disks and studied the forces acting on cylinders translating in an infinite medium and axisymmetrically in tubes. Thiessen and Krantz[5] observed different settling velocities in different experiments using the falling needle viscometer and indicated that the axisymmetric falling cylinders are not necessarily experiencing the highest settling velocity (minimum drag). Wehbeh *et al.*[7] measured the drag of long cylinders of various radii settling in closed and open-ended tubes. When the tube was closed, as expected, the discrepancy between the experimental data and the one-dimensional solution[1–3] decreased as the cylinder's length to radius ratio increased. This was not the case, however, when Wehbeh *et al.*[7] compared their experimental data for the open tube with Happel and Brenner's[8] analytical solution for flow in a concentric annulus. In fact, in the latter case, the discrepancy between the experimental data and the theoretical predictions increased as the cylinder's length to radius ratio increased. As we shall see, this discrepancy disappears once the particle induced through flow is accounted for.

Piercy *et al.*[9] derived an analytical solution for the flow field in an eccentric annulus. Their solution is reproduced in White.[10] For a given radii ratio and pressure gradient, Piercy *et al.*[9] observed that the flow-rate increases monotonically as the eccentricity increases. In other words, the drag force decreases as the eccentricity increases. The situation is somewhat different in the case of the translating particle. Close proximity of the cylindrical particle to the tube's wall results in high drag. Therefore, there is an ''optimal'' eccentricity for which the drag is minimized.[4,5] Prior workers focused on eccentrically translating particles in a closed tube. Here, we extend the analysis to include open tubes.

This paper is organized as follows. In Sec. II, we formulate the mathematical model. Section III extends the well-known solution for a long cylinder translating in a closed tube to the case when the tube is open and subjected to an external pressure gradient. By accounting for the fact that the cylinder acts as a leaky piston, we obtain a simple analytical expression for the drag that is in excellent agreement with experimental observations. In Sec. IV, we derive a solution for the case of a guided cylinder translating eccentrically in an open tube and determine the drag and torque as functions of the eccentricity. Not surprisingly, in the eccentric case, the cylinder will experience torque that (unless guided) would prevent it from maintaining coaxial motion. Section V describes a numerical algorithm that allows one to efficiently compute the flow field around a finite guided cylinder moving in a long tube. Unguided, eccentric moving cylinders are studied numerically and experimentally in Sec. VI. Section VII summarizes our conclusions.

[a]Author to whom correspondence should be addressed; electronic mail: bau@seas.upenn.edu

 

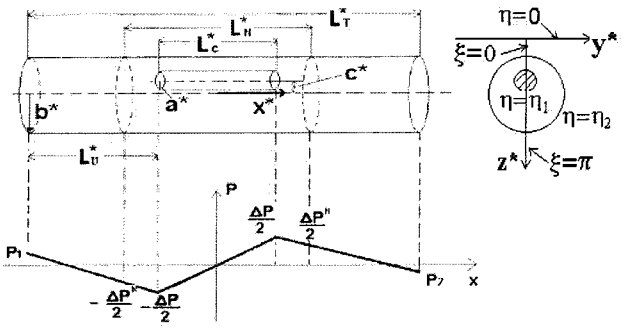


FIG. 1. A schematic depiction of the mathematical model.

## II. MATHEMATICAL MODEL

Consider a long cylindrical particle of radius $a^*$ and length $L_C^*$ translating axially with a constant velocity $U^*$ in a long tube of radius $b^*(>a^*)$ and length $L_T^*(\gg L_C^*)$ (Fig. 1). The superscript (*) denotes dimensional quantities that will later be made dimensionless. The cylinder's axis is displaced distance $c^*$ from the tube's axis, and its upstream end is located distance $L_U^*$ downstream from the tube's entrance. The cylinder's axis is parallel to the tube's axis. The coordinate $x^*$ is aligned with the tube's axis and points in the direction of the cylinder's motion. We use a laboratory frame of reference with the origin of the coordinate system coinciding with the instantaneous center of the particle. The cylinder occupies the interval $|x^*| \leqslant L_C^*/2$. When the tube is open, the upstream and downstream ends of the tube are maintained, respectively, at pressures $P_1^*$ and $P_2^*$. In all the cases considered here, $L_U^* \gg b^*$ and $(L_T^* - L_U^* - L_C^*) \gg b^*$. In other words, the tube is sufficiently long to accommodate fully developed (parabolic) velocity profiles some distance upstream and downstream of the particle. We will comment on the length needed to establish a fully developed profile later in the paper. The particle's motion can be induced by external gravitational, magnetic, and/or electric force fields.

We are concerned with small Reynolds numbers ($\mathrm{Re} = U^* b^*/\nu \ll 1$), where $U^*$ is the particle's velocity and $\nu$ is the fluid's kinematic viscosity. The fluid motion is described by the dimensionless Stokes and continuity equations,

$$\nabla^2 \mathbf{u} = \nabla P \tag{1}$$

and

$$\nabla \cdot \mathbf{u} = 0. \tag{2}$$

In the above, $\mathbf{u}$ is the velocity vector and $P$ is the pressure. Bold letters represent vectors. We use the cylinder's velocity $U^*$ as the velocity scale, the tube's radius $b^*$ as the length scale, and $\mu U^*/b^*$ as the pressure scale. The symbol $u$ is the velocity component in the axial ($x$) direction. On the cylinder's surface, $u=1$, and at the tube's wall, $u=0$.

Mass conservation requires that

$$\frac{1}{\pi}\int_{A_g} u\, dA + a^2 = \chi \quad \left(-\frac{L_C}{2} < x < \frac{L_C}{2}\right), \tag{3}$$

where $\chi$ is the cross-sectionally averaged velocity and the integration is carried out over the cross-sectional area $A_g$ between the particle and the tube. In general, $\chi$ is not *a priori* known, and it needs to be determined as part of the solution process. When $L_T \to \infty$ and/or one of the tube's ends is closed, $\chi = 0$.

In the foregoing, we divide the tube into the upstream region, the particle's region, and the downstream region. The particle's region ($L_N > L_C$) is sufficiently long so that one can assume there is a parabolic, fully developed profile at $|x| = L_N/2$. The pressure distribution as a function of $x$ in these three regions is depicted schematically in Fig. 1, where, without loss of generality, we specified $P=0$ at $x=0$,

$$P\left(\pm\frac{L_C}{2}\right) = \pm\frac{\Delta P}{2} \quad \text{and} \quad P\left(\pm\frac{L_N}{2}\right) = \pm\frac{\Delta P^N}{2}.$$

We can relate the average velocity $\chi$ to the pressure drop

$$P_1 - P_2 + \Delta P = 8\chi(L_T - L_C), \tag{4}$$

where $\Delta P$ is the pressure difference over the particle's region. When the tube is closed or of an infinite length, $\chi = 0$,

$$P\left(x < -\frac{L_C}{2}\right) = -\frac{\Delta P}{2} \quad \text{and} \quad P\left(x > \frac{L_C}{2}\right) = \frac{\Delta P}{2}.$$

In order to obtain $\Delta P$, we need to compute the flow field around the particle. We first consider the limiting cases of both concentric and eccentric long cylinders $L_C \gg (1-a)$, which we solve analytically. Subsequently, we comment on how one can compute numerically the flow field in the case of a finite length cylinder.

## III. LONG, CONCENTRIC CYLINDER

The calculation of the flow field around and the drag on a long, concentric cylinder settling in a closed tube is of interest in the analysis of needle viscometers. Using small gap approximation, numerous researchers[1–3] have produced the solution when $\chi = 0$. Here, we provide the straightforward extension for the case of $\chi \neq 0$. We use cylindrical coordinates with the radius $r$ originating at the tube's axis. The velocity distribution far from the cylinder's ends ($|x| < L_C/2$) is

$$u = \frac{1}{4}\left(-\frac{dP}{dx}\right)\left[1 - r^2 - \frac{\ln(r)}{\ln(a)}(1-a^2)\right] + \frac{\ln(r)}{\ln(a)}. \tag{5}$$

The pressure gradient is obtained from mass conservation,

$$\left(-\frac{dP}{dx}\right) = \frac{-4(1-a^2+2\chi\ln(a))}{(a^4-1)\ln(a) - (1-a^2)^2}. \tag{6}$$

The dimensionless viscous drag acting on the cylinder's surface is

$$D_s = \frac{1}{4}\left(-\frac{dP}{dx}\right)\left(-2a^2 + \frac{a^2-1}{\ln(a)}\right) + \frac{1}{\ln(a)}. \tag{7}$$

In the above, the force was normalized with $2\pi\mu U^* L_C^*$. Neglecting edge effects, to the first order, the pressure drop across the length of the cylinder is $(-dP/dx)L_c$ and the total force (due to both viscous and pressure effects) that is needed to maintain the cylinder's velocity is

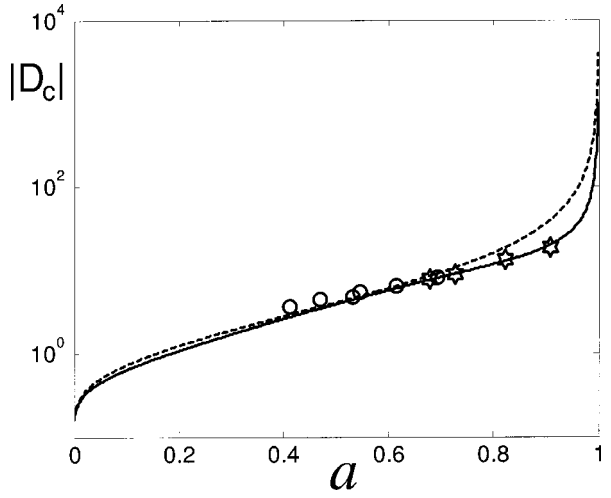


FIG. 2. The dimensionless drag as a function of the cylinder's radius ($a$). The solid line, dashed line, and symbols correspond, respectively, to our analytical solution for a cylinder translating in an open tube, Happel and Brenner's expression for the flow in a concentric annulus, and Wehbeh's experimental data. The circles and stars correspond, respectively, to unguided and guided cylinders.

$$D_C=\frac{1}{4}\left(-\frac{dP}{dx}\right)\left(\frac{a^2-1}{\ln(a)}\right)+\frac{1}{\ln(a)}. \tag{8}$$

In the above, we use the subscript $C$ to indicate the cylinder is translating concentrically. Alternatively, we can write expression (8) in terms of $\chi$,

$$D_C=\frac{(1+a^2)-2\chi}{1-a^2+(1+a^2)\ln(a)}. \tag{9}$$

Figure 2 depicts the absolute value of the dimensionless drag as a function of the cylinder's radius ($a$). The solid line, symbols, and dashed line correspond, respectively, to the prediction of Eq. (9), Wehbeh *et al.*[7] experiments (circles and stars), and the solution for the flow in a concentric annulus (with which Wehbeh *et al.*[7] compared their experimental data). Witness that as $a$ increases, the discrepancy between the experimental data and our theoretical solution decreases. The discrepancy between experiment and theory at small $a$ values can be attributed to the end effects that were not accounted for in the theory.

## IV. LONG, GUIDED ECCENTRIC CYLINDER

Piercy *et al.*[9] solved analytically the case of fully developed flow in an eccentric annulus ($U^*=0$, $\chi^*\neq 0$). We extend their solution to the case of the translating cylinder. For the readers' convenience, we adopt the Piercy *et al.* notation. We assume that the cylinder is guided so that its axis remains parallel to the tube's axis.

The geometry suggests the use of bi-cylindrical coordinates.[11] This coordinate system consists of two orthogonal families of circles. One family of circles corresponds to constant value $\eta$ coordinates ($\eta_1\geqslant\eta\geqslant\eta_2$). The cylinder's and tube's surfaces correspond, respectively, to $\eta=\eta_1$ and $\eta=\eta_2$. The second family of circles corresponds to constant $\xi$ ($-\pi\leqslant\xi\leqslant\pi$) coordinates. The relationship between the Cartesian coordinates $(y,z)$ transverse to the tube's axis and the bi-cylindrical coordinates $(\xi,\eta)$ is given by

$$y+iz=M\tan(\tfrac{1}{2}(\xi+i\eta)), \tag{10}$$

where

$$M=(F^2-1)^{1/2},\quad F=\frac{1-a^2+c^2}{2c},$$

$$\eta_1=\frac{1}{2}\ln\frac{F-c+M}{F-c-M},\quad \text{and}\quad \eta_2=\frac{1}{2}\ln\frac{F+M}{F-M}.$$

The axial velocity is

$$u(\xi,\eta)=\psi-\frac{1}{4}\left(-\frac{dP}{dx}\right)M^2\left(\frac{\cosh\eta-\cos\xi}{\cosh\eta+\cos\xi}\right)+\frac{\eta-\eta_2}{\eta_1-\eta_2}, \tag{11}$$

where

$$\psi=\left(-\frac{dP}{dx}\right)M^2\left[c_0+c_1\eta+\sum_{n=1}^{\infty}(-1)^n\frac{e^{-n\eta_1}\coth\eta_1\sinh n(\eta-\eta_2)-e^{-n\eta_2}\coth\eta_2\sinh n(\eta-\eta_1)}{\sinh n(\eta_1-\eta_2)}\cos(n\xi)\right],$$

$$c_0=\frac{\eta_1(1-2\coth\eta_2)-\eta_2(1-2\coth\eta_1)}{4(\eta_2-\eta_1)},\quad \text{and}\quad c_1=\frac{\coth\eta_2-\coth\eta_1}{2(\eta_2-\eta_1)}.$$

The flow rate is

$$Q=\frac{\pi}{8}\left(-\frac{dP}{dx}\right)\left(1-a^4-\frac{4c^2M^2}{\eta_1-\eta_2}-8c^2M^2\times\sum_{n=1}^{\infty}\frac{n\exp(-n(\eta_1+\eta_2))}{\sinh(n(\eta_1-\eta_2))}\right)+\pi\left(\frac{Mc}{\eta_1-\eta_2}-a^2\right). \tag{12}$$

The pressure gradient is

$$\left(-\frac{dP}{dx}\right)=\frac{8\left(\chi+\dfrac{Mc}{\eta_2-\eta_1}\right)}{1-a^4-\dfrac{4c^2M^2}{\eta_1-\eta_2}-8c^2M^2\Sigma_{n=1}^{\infty}\dfrac{ne^{-n(\eta_2+\eta_1)}}{\sinh n(\eta_1-\eta_2)}}. \tag{13}$$

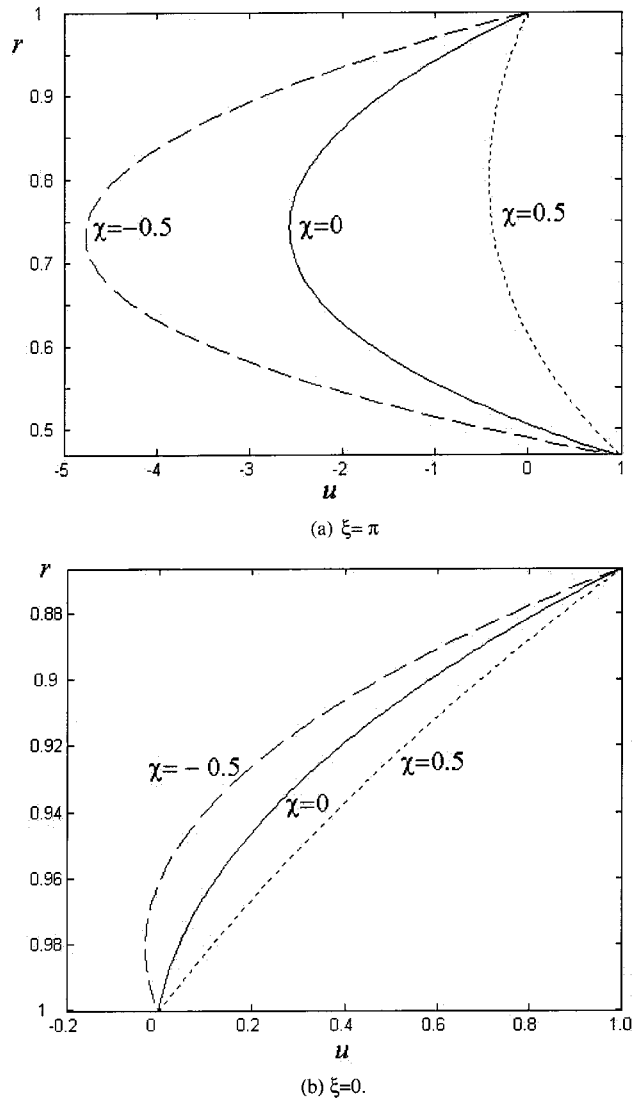


FIG. 3. The axial velocities $u(\pi,\eta)$ (a) and $u(0,\eta)$ (b) at $x=0$ are depicted as functions of the radial coordinate $r$ when $\chi=-0.5$, 0, and 0.5. The relative eccentricity $e=0.2$ and the radii ratio $a=2/3$.

The viscous force (normalized with $2\pi\mu\, U^*L_c^*$) that acts on the cylinder's surface is

$$D_S=\frac{-\mu L_c^*\int_{-\pi}^{\pi}\left(\frac{\partial u^*}{\partial \eta}\right)_{\eta=\eta_1} d\xi}{2\pi\mu U^*L_c^*}$$

$$=-\frac{1}{2}\left(-\frac{dP}{dx}\right)\left(\frac{Mc}{\eta_2-\eta_1}+a^2\right)-\frac{1}{\eta_1-\eta_2}. \qquad (14)$$

The total force (viscous and pressure forces combined) that is needed to maintain the cylinder's motion is

$$D_E=-\frac{1}{2}\left(-\frac{dP}{dx}\right)\left(\frac{Mc}{\eta_2-\eta_1}\right)-\frac{1}{\eta_1-\eta_2}. \qquad (15)$$

In the above, we used subscript $E$ to indicate an eccentric case.

Figure 3 depicts the axial velocity as a function of the radial coordinate $r$ (centered on the tube's axis) when $\chi=0$, $\chi=0.5$, and $\chi=-0.5$. In Fig. 3(a), $\xi=\pi$, and in Fig. 3(b), $\xi=0$. Both $\xi=0$ and $\xi=\pi$ correspond to $x=0$. The radii ratio $a=2/3$ and the relative eccentricity (the eccentricity normalized with the gap's height $e=c/(1-a)$), $e=0.2$. To enhance visibility, Figs. 3(a) and 3(b) have different radial scales.

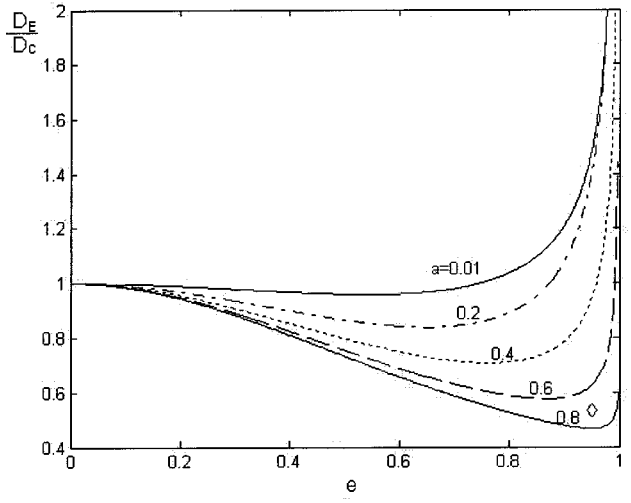


FIG. 4. The normalized drag force is depicted as a function of the relative eccentricity when the radii ratios are $a=0.01$, 0.2, 0.4, 0.6, and 0.8. $\chi=0$. The diamond corresponds to an experimental data point (Ref. 5).

The force $D_E$ that is needed to maintain the cylinder's motion is depicted in Fig. 4 as a function of the relative eccentricity for cylinders of various radii $a=0.01$, 0.2, 0.4, 0.6, and 0.8 settling in a closed tube ($\chi=0$). The force was normalized with the force that would have existed in the case of a concentric cylinder with the same radii ratio. Witness that as the eccentricity increases, the force decreases, attains a minimum, and then increases again. When $e\to 1$, $|D_E|\to\infty$. When the cylinder's radius is relatively small, the effect is not very pronounced. When the cylinder's radius is large, the reduction in the drag may be quite significant. For example, when $a=0.8$, the minimum drag is attained at a relative eccentricity of 0.95, and it is about 47% of the drag

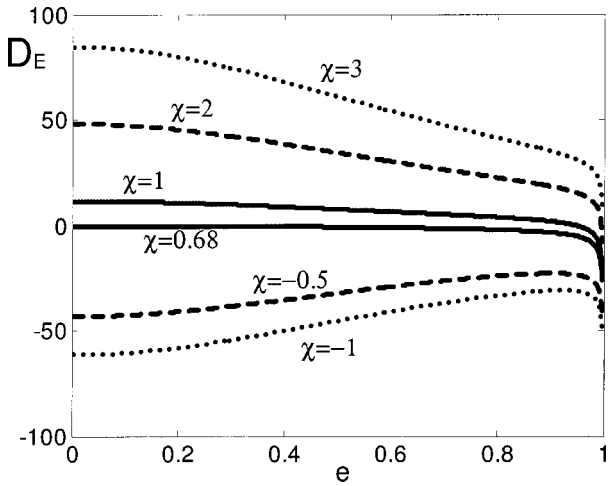


FIG. 5. The drag force ($D_E$) is depicted as a function of the relative eccentricity when $\chi=-1$, $-0.5$, 0.68, 1, 2, and 3. The radii ratio $a=0.6$.

in the corresponding concentric case. We denote the eccentricity at which the drag attains a minimum as the optimal eccentricity $e_o$.

We were not able to find experimental data that documents explicitly the drag as a function of the eccentricity. Thiessen and Krantz[5] dropped a cylinder of radius $a \sim 0.8$ in a tube. The settling velocity was repetitively measured in a sequence of seemingly identical experiments with the only possible variable being the cylinder's initial position. We assume that the highest velocity is attained by a cylinder settling at nearly the optimal eccentricity. By comparing this velocity to the settling velocity of a concentrically settling cylinder, we obtain an estimate of the minimal drag. The experimental data point (symbol) is included in Fig. 4, and it is located slightly above the theoretical prediction. The difference may be attributed to possible end effects that were not accounted for in the theory.

Figure 5 depicts the force $D_E$ as a function of the relative eccentricity ($e$) when $a=0.6$ and $\chi=-1$, $-0.5$, 0.68, 1, 2, and 3. When $\chi<0.68$, the force is negative for all eccentricities. As the eccentricity increases, the absolute value of the force decreases, attains a minimum, and then increases again similarly to the case of $\chi=0$ (Fig. 4). As $\chi$ increases above 0.68, the direction of the drag force acting on the cylinder reverses. In other words, once the through flow is sufficiently high, it is necessary to apply a force in a direction opposite to the cylinder's direction of motion to keep the cylinder from increasing its velocity. In this case, the drag acting on the concentric cylinder will be positive. As the eccentricity increases, $D_E$ decreases monotonically. At a certain eccentricity ($e_o$), $D_E=0$. For example, when $a=0.6$, $c=0.3$, and $\chi=0.76$, the cylinder will move at a velocity of one without any external force being applied to the cylinder itself ($D_E=0$). Further increases in the eccentricity will result in a negative $D_E$. As the cylinder gets closer to the conduit's wall, larger forces are needed to sustain its motion. As $e \to 1$, $D_E \to -\infty$.

Figure 6 depicts the optimal eccentricity ($e_o$) as a function of $\chi$ when $a=0.6$. When $\chi$ increases, the "optimal" eccentricity that corresponds to the smallest force $|D_E|$ decreases, attains a minimum, and then increases again. When $0.63<\chi<0.68$, $|D_E|$ attains its smallest value when the cylinder is concentric. As $|\chi|$ increases, the "optimal eccentricity" increases and approaches the value of 1. The branch $\chi>0.68$ corresponds to $D_E=0$.

Heretofore, we have assumed that the cylinder is guided. An interesting question is whether an unguided cylinder will translate parallel to the tube's axis. To answer this question, we calculate the contribution of the shear stresses to the torque (normalized by $\mu U^* L_C^*$) acting on the cylinder. There is also a normal stress contribution to the torque which cannot be calculated from our approximate theory, but which we will include when we solve the problem numerically. The dimensionless torque ($T_s$) resulting from the shear stresses is

$$
\begin{aligned}
T_s &= -\int_{-\pi}^{\pi} \left(\frac{\partial u}{\partial \eta}\right)_{\eta=\eta_1} (z - M\coth\eta_1)\, d\xi \\
&= -2\pi M^3 \left(-\frac{dP}{dx}\right)\Bigg[c_1 + \sum_{n=1}^{\infty}\Bigg((-1)^n n e^{-n\eta_1}\Bigg[e^{-n\eta_1}\coth\eta_1\coth n(\eta_1-\eta_2) - e^{-n\eta_2}\frac{\coth\eta_2}{\sinh n(\eta_1-\eta_2)}\Bigg]\Bigg) \\
&\quad - \frac{1}{32\cosh\eta_1\sinh^2\eta_1}\Bigg[\coth^3\frac{\eta_1}{2}(\cosh 3\eta_1 - 6\cosh 2\eta_1 + 15\cosh\eta_1 - 10) - \tanh\frac{\eta_1}{2}(\cosh 3\eta_1 + 2\cosh 2\eta_1 \\
&\quad + 7\cosh\eta_1 + 6)\Bigg]\Bigg] - \frac{2M\pi(1-\coth\eta_1)}{\eta_1-\eta_2} + M\pi\coth\eta_1\left(-\frac{dP}{dx}\right)\left(\frac{Mc}{\eta_2-\eta_1} + a^2\right). \qquad (16)
\end{aligned}
$$

In the above, $(z - M\coth\eta_1)$ is the distance from a point on the cylinder's surface to a plane that is normal to $z$ and passes through the cylinder's axis. The expression for $T_s$ is applicable only when the cylinder's axis is parallel to the tube's axis. Figure 7 depicts the torque $T_s$ as a function of the eccentricity ($e$) when $\chi=-1$, 0, and 1 and $a=0.5$. The angle of attack is taken to be positive ($\theta>0$) when the downstream end of the cylinder tilts towards the tube's center (refer to Fig. 1). When $T_s>0$ ($T_s<0$), the torque tends to rotate the cylinder so as to form a positive (negative) angle of attack. Once the cylinder has been tilted, one would expect the presence of radial forces.

## V. NUMERICAL SIMULATION

To account for end effects, we solve the problem numerically with the finite element package Femlab.[12] We consider only flat-ended cylinders. In Secs. V A and V B, we describe simulation results for the concentric and guided eccentric particles. In Sec. VI, we discuss briefly the case of the unguided eccentric cylinder.

Unfortunately, the net flow $\chi$ through the tube is not known *a priori*, and it needs to be obtained as part of the solution process. A brute-force approach would be to simulate the entire length of the tube. When the tube length

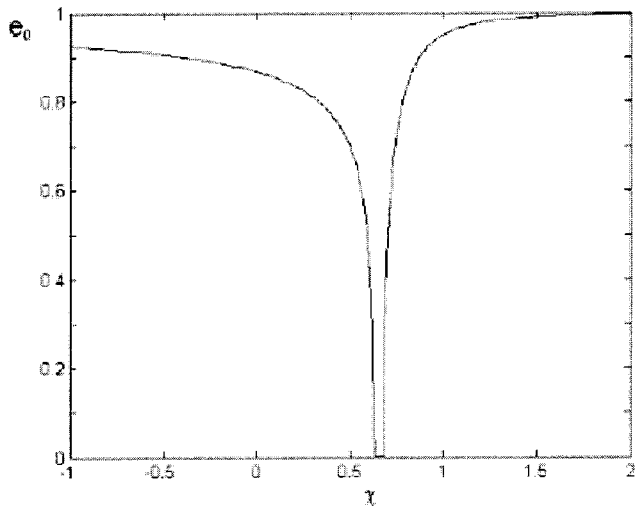


FIG. 6. The optimal eccentricity ($e_o$) at which the absolute value of the drag, $|D_E|$, attains a minimum is depicted as a function of $\chi$. The radii ratio $a=0.6$.

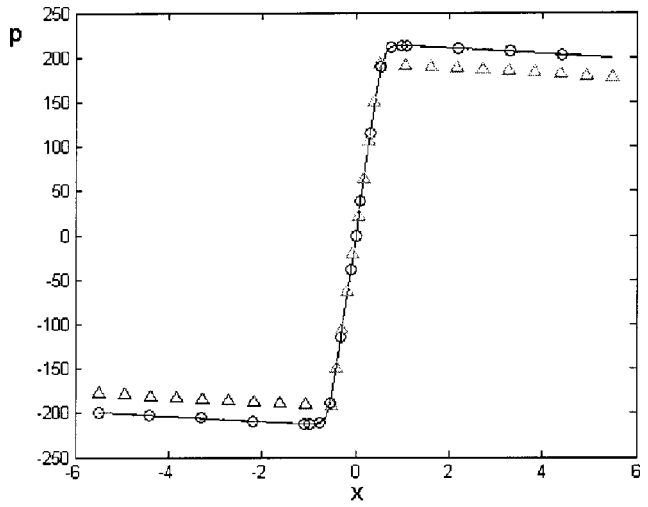


FIG. 8. The pressure distribution along the tube length $|x|<L_N$. The solid line, the circles, and the upper triangles correspond, respectively, to the results of the brute-force numerical simulation, the superposition technique and the analytical solution. $L_C=1$, $L_N=11$, $e=0$, $L_T=140$, $a=0.8$, and $P_1=P_2=0$.

$L_T \gg L_C$, a very large number of elements may be needed. Such a large number of elements may tax heavily computer resources. Happily, there is an alternative that we outline below.

We wish to carry out calculations only in the region $|x|<L_N/2$, where $L_N$ is sufficiently large that the flow at $|x|=L_N/2$ can be assumed to be fully developed. To do so, we need to specify appropriate boundary conditions at $|x|=L_N/2$. Since the problem is linear, one can use the method of superposition. Briefly, we denote the pressure at the upstream and downstream ends $x=\pm L_N/2$ as $\pm\Delta P^N/2$. $L_N$ is selected sufficiently large so that one can assume Poiseuille flow when $x \geqslant |L_N/2|$. Accordingly,

$$P_1-P_2+\Delta P^N=8\chi(L_T-L_N). \tag{17}$$

Next, we solve two problems for the velocities $\mathbf{u}_1$ and $\mathbf{u}_2$. Both $\mathbf{u}_1$ and $\mathbf{u}_2$ satisfy the Stokes and continuity equations (1) with nonslip boundary conditions at the tube's wall and an axial velocity component of magnitude one on the cylinder's surface. Both the tube's and the cylinder's walls are impermeable. To complete the problem specification, we specify, respectively, $u_1=2\chi_1(1-r^2)$ and $u_2=2\chi_2(1-r^2)$ as the velocity boundary conditions at $|x|=L_N/2$ in the problems for $\mathbf{u}_1$ and $\mathbf{u}_2$. In the above, $\chi_1$ and $\chi_2$ are arbitrarily chosen. We then solve these two problems independently. The solution to the actual problem is constructed by the superposition

$$\mathbf{u}=C_1\mathbf{u}_1+C_2\mathbf{u}_2. \tag{18}$$

Since the velocity $u$ on the cylinder's surface equals unity, the coefficients $C_1$ and $C_2$ must satisfy

$$C_1+C_2=1. \tag{19}$$

The superposed pressures must satisfy the pressure condition of the original problem,

$$C_1\Delta P_1^N+C_2\Delta P_2^N=8\chi(L_T-L_N), \tag{20}$$

where

$$\chi=C_1\chi_1+C_2\chi_2. \tag{21}$$

To verify that the superposition technique, indeed, works, we solved the same problem with the brute-force (simulating the entire length of the tube) and superposition approaches. For example, when $L_T=140$, $L_C=1$, $a=0.8$, $P_1=P_2=0$, and $e=0$, the superposition method (with $L_N=11$, $\chi_1=1$, and $\chi_2=-1$) predicts $\Delta P_1^N=-289.7$, $\Delta P_2^N=1956.4$, $C_1=0.69$, $C_2=0.31$, and $\chi=0.387$. The brute-force approach predicts $\chi=0.380$ in good agreement with the value that was obtained with the superposition method. Both the velocity profiles and the pressure distributions computed with the superposition method and the brute-force approach were in excellent agreement. Figure 8 depicts the pressure distribution along the conduit's axis. The solid line and circles correspond, respectively, to the brute-force and superposition solutions. The upward triangles correspond to the

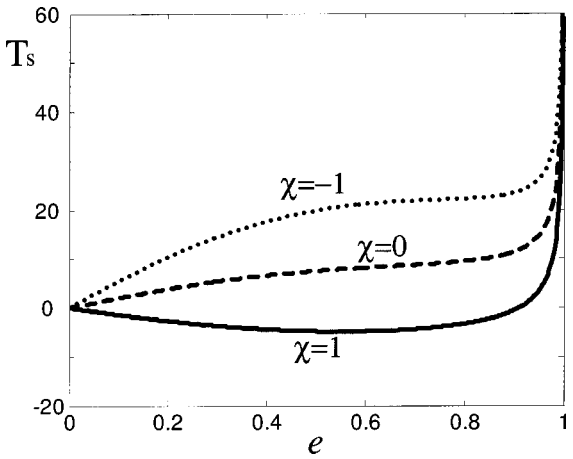


FIG. 7. The torque resulting from the axial shear on the cylinder's surface as a function of the eccentricity. Positive torque causes the cylinder's downstream end to tilt towards the tube's center. The radii ratio $a=0.5$.

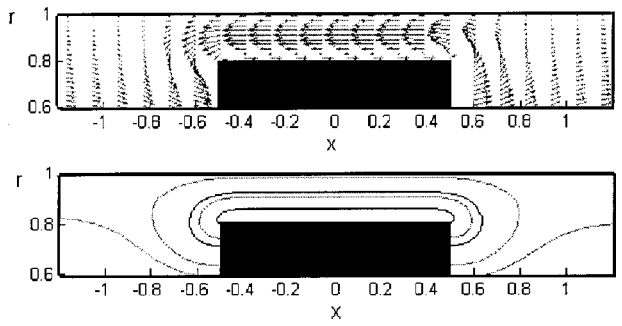


FIG. 9. The velocity field (upper half) and the streamlines (lower half) in the cylinder's vicinity. The simulation's conditions are the same as in Fig. 8.

approximate analytical prediction [Eq. (6)]. The analytical approximation underestimates somewhat the pressure drop due to unaccounted end effects.

### A. Finite concentric cylinder in a long tube

Figure 9 depicts the velocity vector field (upper half of the figure) and the streamlines (lower half) around the cylinder when $P_1=P_2=0$ and $L_T=140$. For clarity, only part of the cylinder is shown $(0.6<r<1)$. Some of the fluid displaced by the cylinder is pumped through the annulus, and some circulates back to occupy the space behind the advancing cylinder.

Another issue of interest is how far from the cylinder the velocity profile becomes parabolic and fully developed. When $a=0.8$, $c=0$, $L_c=1$, and $\chi=0.387$, Fig. 10 depicts the maximum value of the velocity in each cross section as a function of the axial distance $x$. We define the development length as the distance until the maximum velocity at the tube's center attains the value of $|[u(x,0)/2\chi]-1|<0.01$. The development distance in Fig. 10 is about 1.64. This development length is slightly larger than the value estimated by Katopodes *et al.*[13] for a leakless piston. Katopodes *et al.*[13] used Papkovich–Fadle eigenfunctions to study the transition from a uniform velocity profile to a fully developed, parabolic profile. The decay to the parabolic profile is described

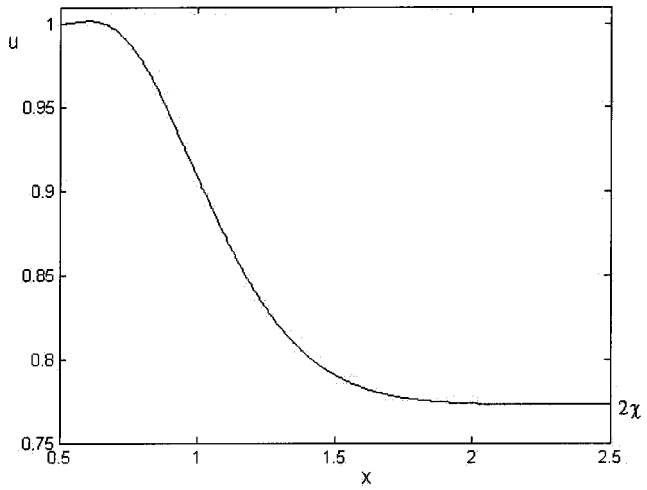


FIG. 10. The centerline velocity $u$ at $y=0$ is depicted as a function of $x$. $L_c=1$, $L_N=11$, $e=0.8$, $L_T=140$, $a=0.8$, and $P_1=P_2=0$.

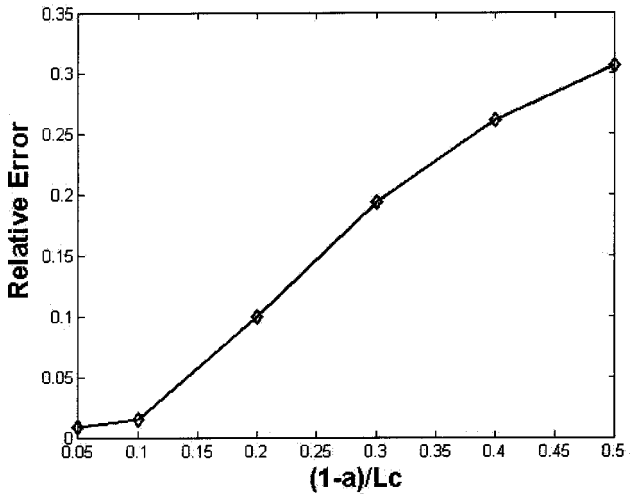


FIG. 11. The relative error between the one-dimensional theory and the three-dimensional numerical results as a function of $(1-a)/L_c$, $L_c=1$, $L_N=5$, and $L_T=140$.

by an infinite series with terms of the form $\exp(-\lambda_n x)f_n(r)$. As $x$ increases, the decay is governed by the smallest eigenvalue. Consistent with our previous definition, we define the development length as $x_D\sim 4.6/\lambda_1$. For a cylindrical barrel, $\mathrm{Re}(\lambda_1)\sim 4.463$ and $x_D\sim 1.03$. This suggests a fairly fast adjustment, within one radius of the tube. Figure 10 suggests that one can select $L_N\sim L_C+4$ without a significant loss of precision.

Figure 11 depicts the relative difference between the analytically and numerically computed total drag as a function of $(1-a)/L_c$. As $(1-a)/L_c$ increases, the significance of the end effects increases and so does the relative error. The relative discrepancy is, respectively, 0.9% and 31% when $(1-a)/L_c=0.05$ and 0.5. Finally, we compare the dimensionless drag force with Davis'[6] calculations. Davis used an array of disks to approximate a finite, axisymmetric cylinder translating in a tube. Davis defined the dimensionless drag force as

$$F_D=\frac{\text{Drag}}{16\mu U^* a^*}. \tag{22}$$

Table I displays the numerically computed drag using the superposition technique and Davis' results when $L=L_c/2a=0.5$ and $a^{-1}=1.5$, 2, 3, and 5. As the cylinder's diameter decreases, the results from Davis' approximate analysis agree better with our numerical calculation.

TABLE I. The comparison of the values of $F_D$ predicted by our calculations and Davis' approximate results $(L=0.5)$.

| | $1/a$ | | | |
|---|---|---|---|---|
| $F_D$ | 1.5 | 2 | 3 | 5 |
| Superposition | 25.6069 | 8.0068 | 3.4603 | 2.0955 |
| Davis[a] | 26.1970 | 7.9348 | 3.4364 | 2.0877 |

[a]Reference 6.

### B. Guided, eccentrically placed cylinder

We carried out a few three-dimensional numerical computations for a long, eccentric cylinder translating in a tube. Femlab's[12] predictions for the total drag were in reasonable agreement with the analytical predictions of the two-dimensional theory. For example, when $a=0.7$, $c=0.2$, $L_C=9$, and $L_T=10$, the two-dimensional analytical solution predicts $\{D_E, T_S\}=\{-4.0, 5.5\}$ while the computational results are $\{-3.7, 5.2\}$.

## VI. UNGUIDED ECCENTRICALLY PLACED CYLINDER

When the eccentrically positioned cylinder is not guided, the torque acting on the cylinder will cause it to rotate around its center of mass. The rotation gives rise to radial forces that will tend to move the cylinder either towards or away from the tube's center. Although the prediction of the cylinder's trajectory is not the prime objective of this paper, we carried out a few computations and experiments to gain some insights into the cylinder's trajectory.

We carried out both two- and three-dimensional numerical simulations. The three-dimensional simulations were carried out with Femlab while the two-dimensional simulations were carried out with the particle mover.[14] Femlab has the advantage of providing a friendly user interface that allows easy coding of the geometry under consideration. Unfortunately, Femlab cannot handle moving interfaces. In order to compute the cylinder's trajectory with Femlab, it would have been necessary to remesh the grid at nearly every time step—a very time consuming proposition, indeed. In contrast, the particle mover handles moving interfaces elegantly; but it lacks a graphical user interface, and the incorporation of the geometry under consideration would constitute a cumbersome coding exercise. As a compromise, we used Femlab to calculate the torque and the radial force in a three-dimensional setting and the particle mover to gain qualitative insight into the cylinder's trajectory in a two-dimensional setting.

Figures 12(a) and 12(b) depict, respectively, the torque and radial force as functions of the angle of attack ($\theta$) when the tube is closed (solid line) and open with zero pressure difference between the inlet and the exit (dashed line). The torque ($T$) is positive when it tends to increase $\theta$. The radial force is considered to be positive in the $y$ direction (i.e., towards the tube's center). In Fig. 12, $a=0.25$, $L_C=1$, $L_T=10$, and the relative eccentricity $c=0.2$. The directions and magnitudes of the torque and radial force are functions of position (eccentricity).

Next, we anticipate the chain of events when a cylinder initially placed eccentrically with angle $\theta=0$ settles in a closed tube. As a result of the eccentric position and nonuniform shear stress distribution along the cylinder's surface, torque will act on the cylinder. Consequently, the cylinder will rotate to form a positive angle of attack ($\theta>0$). Once the cylinder is tilted with respect to the direction of the flow, the nonuniform pressure distribution around the cylinder gives rise to a radial force, and the cylinder migrates towards the tube's center. Since the torque and radial force depend on the location of the cylinder, Fig. 12 tells us only that an initially coaxially aligned cylinder will rotate and migrate towards the tube's center. We speculate that once the cylinder crosses the centerline, the direction of the radial force will reverse and the cylinder's trajectory will oscillate about the tube's axis. To determine whether this is, indeed, the case, we carried out a few simple experiments.

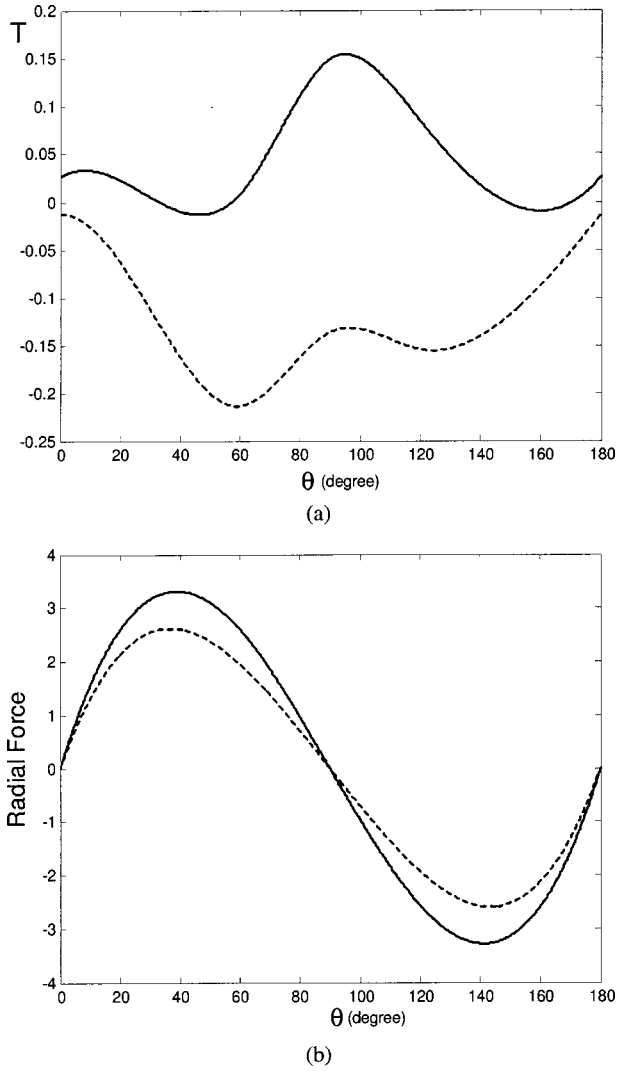


FIG. 12. The torque (a) and radial force (b) acting on an eccentrically positioned cylinder as functions of the angle of attack $\theta$. The solid and dashed lines correspond, respectively, to closed and open ($P_1-P_2=0$) tubes. $a=0.25$, $L_C=1$, $L_T=10$, and $e=0.2$.

We describe briefly only one experiment. The experiment was carried out in a glass tube of $1.27\times10^{-2}$ m radius and 1.5 m length. The tube was filled with glycerin (kinematic viscosity $7.55\times10^{-4}$ m$^2$/s) and positioned vertically. The bottom of the tube was capped with a stopper. A Teflon cylinder (radius, $2.4\times10^{-3}$ m; length, $8\times10^{-3}$ m; and density, $2.16\times10^3$ kg/m$^3$) was dropped vertically off center (with an estimated eccentricity of 0.47). The Reynolds number is estimated to be 0.12. The motion of the cylinder was tracked with a video camera (Nikon CoolPix995). Figure 13 depicts a sequence of frames spaced 5/6 s apart. The images were taken in the tube segment 0.03 m and 0.25 m from the tube's entrance. Since the cylinder had been in motion for a while when frame [Fig. 13(a)] was taken, it is rotated ($\theta>0$).

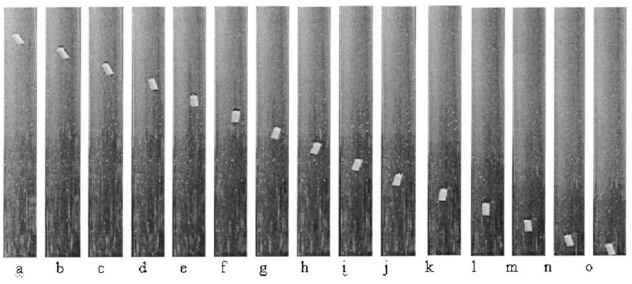


FIG. 13. Photosequences of a Teflon cylinder settling in a closed glass tube filled with glycerin. The frames are spaced at 5/6 s intervals. $a=2.38\times10^{-3}$ m, $b=1.27\times10^{-2}$ m, $L_C=8\times10^{-3}$ m, and $L_T=1.524$ m.

The sequence of images illustrates that the cylinder performs an oscillatory motion about the tube's axis. The photographs are consistent with the theoretical predictions. The experiments seem to suggest that the oscillations about the tube's axis damp out gradually. Due to a lack of adequate equipment, we were not able to conclusively confirm this apparent damping. In order to partially resolve this issue, we resorted to numerical computations.

We used the particle mover to compute the trajectory of a two-dimensional, initially eccentrically positioned slab settling between two parallel plates. Figure 14 depicts the trajectory of a 0.2 wide cylinder of length 1 settling in a conduit of width 1. The slab was initially inserted parallel to the bounding plates at eccentricity 0.5. The Reynolds number is about 0.01. The trajectory depicted in Fig. 14 resembles the experimental observations of Fig. 13. The simulations predict that as the particle settles, its center of mass traces constant amplitude, undamped oscillations about the midplane. The angle of attack changes periodically as a function of the axial distance $x$ (Fig. 15). The simulations suggest, therefore, that the oscillatory motion remains undamped. Clearly, there is a need for definitive experiments to settle the issue.

## VII. CONCLUSIONS

In this paper, we studied theoretically the motion of a cylindrical particle in a tube. The cylinder acts as a leaky piston, inducing circulation around itself and net flow through the tube. The magnitude of the through flow depends on the tube's length, inlet and exit pressures, and the diameters of the cylinder and the tube. Analytical expressions were obtained for the flow field and the drag force as functions of the radii ratio and the eccentricity for the case of a long cylinder translating coaxially. An optimal eccentricity exists at which the drag force is minimized. The analysis predicts that the eccentrically positioned cylinder is subject to torque. Therefore, coaxial motion is possible only when the cylinder is guided. A numerical procedure was outlined to enable efficient calculations of the flow field around finite length, concentric and eccentric cylinders and the forces those cylinders experience. The numerical simulations reveal that an eccentrically placed cylinder experiences both torque and a radial force. As a result, the cylinder will follow an oscillatory trajectory about the tube's axis. This is confirmed with flow visualization experiments. The experiments appear to suggest that the oscillation's amplitude decays. In contrast, two-dimensional numerical simulations indicate constant amplitude oscillations. Hence the issue of whether the oscillatory motion is damped is not resolved in this work.

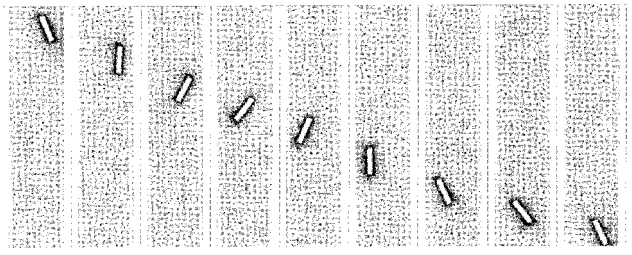

FIG. 14. The computed trajectory of a two-dimensional slab settling between parallel plates.

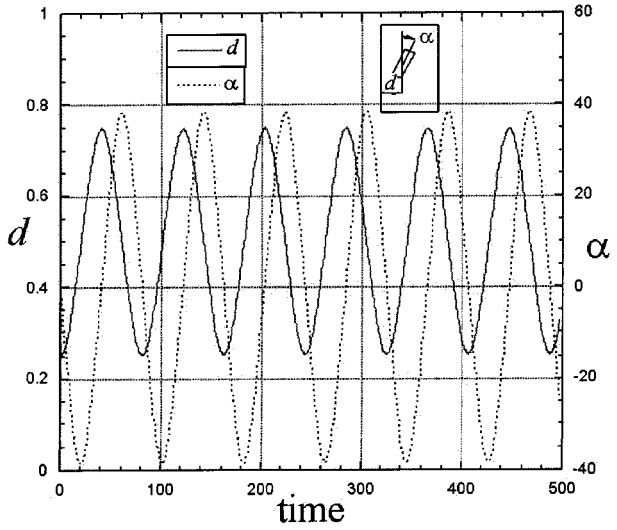


FIG. 15. The distance between the particle's center of mass and the wall $d$ (solid line) and the angle $\alpha$ (dotted line) are depicted as functions of time. The particle's width is 0.2 and its length is 1. The conduit's width is 1.

## ACKNOWLEDGMENT

The work described in this paper was supported, in part, by DARPA (Dr. Anantha Krishnan, Program Director) through a grant to the University of Pennsylvania.

[1] J. Lohrenz, G. W. Swift, and F. Kurata, "An experimentally verified theoretical study of the falling cylinder viscometer," AIChE J. **6**, 547 (1960).
[2] M. C. S. Chen and G. W. Swift, "Analysis of entrance and exit effects in a falling cylinder viscometer," AIChE J. **18**, 146 (1972).
[3] N. D. Cristescu, B. P. Conrad, and R. Tran-Son-Tay, "A closed form solution for falling cylinder viscometers," Int. J. Eng. Sci. **40**, 605 (2001).
[4] M. C. S. Chen, J. A. Lescarboura, and G. W. Swift, "The effect of eccentricity on the terminal velocity of the cylinder in a falling cylinder viscometer," AIChE J. **14**, 123 (1968).
[5] D. B. Thiessen and W. B. Krantz, "Bimodal terminal velocities using the falling needle viscometer," Rev. Sci. Instrum. **63**, 4200 (1992).
[6] A. M. J. Davis, "The use of disks to approximate finite axisymmetric bodies in Stokes flow," Phys. Fluids A **4**, 7 (1992).

[7]E. G. Wehbeh, T. J. Ui, and R. G. Hussey, ''End effects for the falling cylinder viscometer,'' Phys. Fluids A **5**, 25 (1993).
[8]J. Happel and H. Brenner, *Low Reynolds Number Hydrodynamics*, 2nd ed. (Noordhoff, Leyden, 1973), p. 341.
[9]N. A. V. Piercy, M. S. Hooper, and H. F. Winny, ''Viscous flow through pipes with cores,'' Philos. Mag. **15**, 647 (1933).
[10]F. M. White, *Viscous Fluid Flow* (McGraw-Hill, New York, 1974).
[11]P. Moon and D. E. Spencer, *Field Theory Handbook* (Springer-Verlag, New York, 1971).
[12]Femlab is a product of COMSOL AB, Sweden.
[13]F. V. Katopodes, A. M. J. Davis, and H. A. Stone, ''Piston flow in a two-dimensional channel,'' Phys. Fluids **12**, 1240 (2000).
[14]H. H. Hu, N. A. Patankar, and M. Y. Zhu, ''Direct numerical simulations of fluid–solid systems using the arbitrary-Lagrangian–Eulerian technique,'' J. Comput. Phys. **169**, 427 (2001).